

Comparison of real and computer-simulated outcomes of LASIK refractive surgery

Daniel Cano, Sergio Barbero, and Susana Marcos

Instituto de Óptica "Daza de Valdés," Consejo Superior de Investigaciones Científicas, Serrano 121, 28006 Madrid, Spain

Received August 4, 2003; revised manuscript received December 18, 2003; accepted January 14, 2004

Computer simulations of alternative LASIK ablation patterns were performed for corneal elevation maps of 13 real myopic corneas (range of myopia, -2.0 to -11.5 D). The computationally simulated ablation patterns were designed with biconic surfaces (standard Munnerlyn pattern, parabolic pattern, and biconic pattern) or with aberrometry measurements (customized pattern). Simulated results were compared with real postoperative outcomes. Standard LASIK refractive surgery for myopia increased corneal asphericity and spherical aberration. Computations with the theoretical Munnerlyn ablation pattern did not increase the corneal asphericity and spherical aberration. The theoretical parabolic pattern induced a slight increase of asphericity and spherical aberration, explaining only 40% of the clinically found increase. The theoretical biconic pattern controlled corneal spherical aberration. Computations showed that the theoretical customized pattern can correct high-order asymmetric aberrations. Simulations of changes in efficiency due to reflection and nonnormal incidence of the laser light showed a further increase in corneal asphericity. Consideration of these effects with a parabolic pattern accounts for 70% of the clinical increase in asphericity. © 2004 Optical Society of America

OCIS codes: 330.4300, 330.5370, 170.4470, 010.7350.

1. INTRODUCTION

Laser *in situ* keratomileusis (LASIK)^{1,2} is a surgical procedure in which a layer of stromal tissue is removed by laser ablation to change the corneal shape in order to correct the refractive errors of the eye. In this technique, the surgeon uses a microkeratome to cut a hinged flap that is folded back to expose the stroma to the laser radiation. Then a series of laser pulses is delivered onto the tissue to reshape it. Current devices use an argon fluoride excimer laser, emitting ultraviolet radiation of 120–600 mJ/cm² at 193 nm.³ After ablation, the flap is folded over the sculpted stroma.

The purpose of this paper is to compare real and theoretical changes in corneal shape and in optical aberrations produced by LASIK treatments. The real changes were assessed from measurements in a group of patients who underwent LASIK surgery for myopia. The theoretical changes were calculated from computer simulations by using theoretical ablation patterns and preoperative topographical elevation data from the treated corneas.

A LASIK surgery procedure is said to be "standard" when the algorithms programmed into the laser's computer are designed to generate ablation patterns that eliminate defocus and astigmatism (second-order aberrations) without considering effects on higher-order aberrations. Some studies have shown that current standard LASIK treatments for myopia induce important amounts of high-order aberrations.^{4,5} The largest increase occurs for spherical aberration, which is highly correlated with correction. Although only the anterior cornea is ablated, changes on the posterior corneal shape have been reported.⁶ Nevertheless, the change in internal aberrations is much less than that produced in the aberrations of the anterior corneal surface,⁴ and therefore the in-

crease in the total spherical aberration can be attributed mainly to the changes in the anterior corneal shape. A parameter that can be used as a descriptor of the corneal shape is corneal asphericity, which is defined as the asphericity of the conicoid that best fits the corneal shape. A conicoid is a circularly symmetric surface such that the sections along its meridians are conic sections. Asphericity is a parameter that quantifies the deviation of a conicoid from spherical to ellipsoidal, paraboloidal, or hyperboloidal. Smith and Atchison⁷ reported the equation for the primary spherical aberration of a conicoid surface, showing that the higher its asphericity, the higher its primary spherical aberration. (For a corneal refractive index of 1.377, -0.53 asphericity corresponds to 0 spherical aberration and asphericities less than -0.53 correspond to negative spherical aberration). Holladay *et al.*⁸ reported that corneal asphericity increases with current standard LASIK treatments for myopia, consistently with other studies that showed an increase in spherical aberration.^{4,5}

Ablation patterns for refractive surgery are designed with two regions: the optical zone, which is the central area of full refractive correction, and the transition zone, necessary to produce a continuous change of curvature between treated and untreated cornea.^{9,10} The transition zone is important because abrupt changes in corneal curvature may induce excessive epithelial and stromal tissue healing after surgery. An ablation pattern can be described as a continuous mathematical function $f(\rho, \theta)$ representing the thickness of tissue removed at each point (ρ, θ) . Because ablation consists of tissue removal, $f(\rho, \theta)$ cannot be negative at any point.

In a standard LASIK treatment for myopia, the ablation patterns are designed to increase the anterior radius

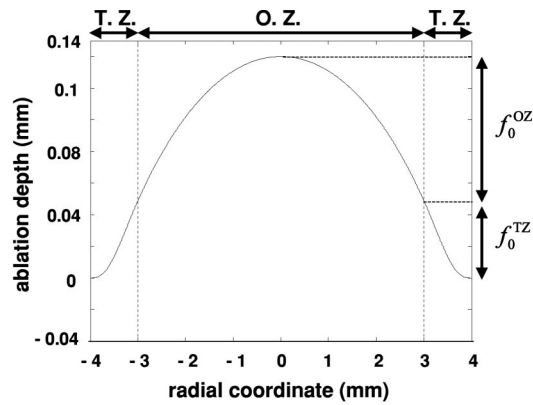


Fig. 1. Munnerlyn pattern correcting for -7 D within a 6-mm-diameter optical zone (O. Z.) for a cornea with 7.8-mm radius of curvature. The ablation pattern within the transition zone (T. Z.) was calculated as a fifth-order polynomial imposing the continuity condition on the function and on its first and second derivatives, between the O. Z. and the T. Z. and between treated and untreated zones.

of curvature in order to reduce the optical power of the eye. Although the algorithms programmed into the laser's computers are proprietary, within the optical zone the generated ablation patterns rely on the equation reported by Munnerlyn *et al.*¹¹ This equation assumes that the preoperative and postoperative corneal surfaces are spherical,

$$f_{\text{Mun}}(\rho) = \sqrt{R_1^2 - \rho^2} - R_1 - \sqrt{R_2^2 - \rho^2} + R_2 + f_0, \quad (1)$$

where R_1 and R_2 are the initial and the desired radius of curvature, respectively. Using the paraxial equation for the optical power of a sphere and assuming that the preoperative and postoperative corneal surfaces are close, R_1 and R_2 are related by

$$S = (n - 1)(1/R_2 - 1/R_1), \quad (2)$$

where S is the optical power correction and $n = 1.377$ is the index of refraction of the cornea.

As shown in Fig. 1, the central ablation depth f_0 is the maximum depth in an ablation pattern designed with the Munnerlyn equation. The central ablation depth f_0 includes the contributions to tissue removal from both the optical and the transition zones (f_0^{OZ} and f_0^{TZ} , respectively). The value f_0^{OZ} is calculated by imposing the continuity condition of the function $f_{\text{Mun}}(\rho)$ at the border between optical and transition zones (Φ is the optical zone diameter). By using Eq. (2) and replacing f_0^{OZ} , we can write Munnerlyn's equation as¹¹

$$f_{\text{Mun}}(\rho) = (R_1^2 - \rho^2)^{1/2} - \left[\left(\frac{R_1(n-1)}{n-1+R_1S} \right)^2 - \rho^2 \right]^{1/2} - \left(R_1^2 - \frac{\Phi^2}{4} \right)^{1/2} + \left[\left(\frac{R_1(n-1)}{n-1+R_1S} \right)^2 - \frac{\Phi^2}{4} \right]^{1/2} + f_0^{\text{TZ}}. \quad (3)$$

Sometimes Munnerlyn's equation is expressed by its parabolic approximation, which is obtained by truncating the Taylor expansion^{12,13}.

$$f_{\text{par}}(\rho) = \frac{4S\rho^2}{3} - \frac{S\Phi^2}{3} + f_0^{\text{TZ}}. \quad (4)$$

In this expression the refractive index n of the cornea has already been replaced by its numerical value, 1.377 (Refs. 10 and 11).

Some researchers have carried out theoretical studies to determine the change in corneal asphericity induced by these standard ablation patterns for myopia. These studies have produced controversial results. Gatinel *et al.*¹⁴ performed a numerical analysis and concluded that Munnerlyn's pattern should produce a decrease in corneal asphericity in corneas with typical preoperative asphericities, which is opposed to the clinical findings. Jiménez *et al.*¹³ carried out exact analytical calculations and found that corneal asphericity should increase after myopic corneal ablation. In this study, these authors used the parabolic approximation of the Munnerlyn equation.

Since in both Munnerlyn and parabolic equations only two parameters are free (the power correction S and the optical zone diameter Φ), astigmatism and high-order aberrations cannot be controlled. However, these ablation patterns can be extended to incorporate astigmatic correction by using a different-power correction for each meridian $S(\theta)$ in formulas (3) and (4). To correct for spherical aberration as well, some authors^{15,16} have proposed ablation patterns in which both preoperative and postoperative corneal shapes are assumed to have a certain asphericity. In these ablation patterns, the asphericity is the new parameter that allows control of the spherical aberration.

Another way to design corneal ablation patterns involves using the wave aberration function $W(\mathbf{r})$ that contains the optical aberrations to be corrected¹⁰:

$$f_{\text{cus}}(\mathbf{r}) = \frac{W(\mathbf{r})}{n-1}, \quad (5)$$

where n is the refractive index of the cornea and $W(\mathbf{r})$ is typically described by a Zernike polynomial expansion. If $W(\mathbf{r})$ includes overall aberrations, the function $f_{\text{cus}}(\mathbf{r})$ describes a customized ablation pattern that could theoretically correct not only defocus and astigmatism but also high-order aberrations. Such surgery requires previous measurements of the individual aberrations by using wave-front-sensing systems.

In this paper we assess the real changes in corneal shape and in optical aberrations produced by a standard LASIK treatment in a group of myopic patients. We also calculate the theoretical corneal shapes and optical aberrations generated by the ablation patterns described above. The theoretical corneal shapes were simulated by subtracting the theoretical ablation patterns from the preoperative topographical elevation data of the treated corneas. The particular parameters of each eye (spherocylindrical correction, aberrations, etc.) were used to calculate the ablation patterns. In this manner, we could perform individual comparisons of the real and the theoretical corneal changes.

In this paper we also assess, using a model from Jiménez *et al.*,¹⁷ how changes in ablation efficiency might in-

crease asphericity. Ablation efficiency quantifies the amount of tissue removed by one laser pulse. Ablation efficiency changes across the cornea because both reflected energy and illuminated area depend on the angle of incidence of the laser light onto the corneal surface.

Understanding the sources of the increase in spherical aberration after use of the current standard myopic procedures is critical to finding optimization strategies for ablation algorithms and to evaluating the prospects of customized-corneal-ablation refractive surgery.

2. METHODS

A. Patients and LASIK Surgery

For this study we used retrospectively both corneal topography data and optical aberrations of 13 eyes from 7 patients who had previously undergone myopic LASIK surgery. Measurements and surgery are described in detail by Marcos *et al.*⁴

Standard LASIK surgery was conducted by using a scanning spot excimer laser (Chiron Technolas 217-C equipped with the PlanoScan program; Bausch & Lomb Surgical, Munich) emitting 50 light pulses per second with a wavelength of 193 nm. The spot diameter varies from 1.0 to 2.0 mm, and the beam energy profile is a truncated Gaussian with 120 mJ/cm² peak fluence. The attempted spherical-equivalent correction ranged from -2 to -11.5 D, and the maximum treated astigmatism was 2.5 D. Optical zone diameters ranged from 4.4 to 7 mm. With this input data, the PlanoScan program calculated central ablation depths between 53 and 143 μm . These surgical parameters are represented for each patient in Table 1. The flap was cut with a Hansatome microkeratome (Bausch & Lomb Surgical), and the laser ablation was guided by an eye tracker. All eyes recovered normally and none was retreated.

B. Measurements of Ocular Aberrations and Corneal Topography

For each patient, ocular aberrations and corneal topography were measured less than 1 mo. before and more than 1 mo. after surgery.

Ocular aberrations were measured at a wavelength of 543 nm by using a laser ray-tracing (LRT) aberrometer developed at the Instituto de Óptica in Madrid, Spain, and described in detail elsewhere.^{18,19} Aberrations were referred to the center of the natural pupil. Measurements were performed for 6.5-mm pupil diameters. The wave aberration function $W(\mathbf{r})$ was described by a

seventh-order Zernike polynomial expansion (sign and normalization followed the Optical Society of America standards²⁰). Anterior cornea heights were measured with a corneal topography system (Atlas Mastervue; Humphrey Instruments–Zeiss, San Leandro, Calif.).

C. “Computer Surgery”

To assess the theoretical changes in corneal asphericity and corneal aberrations induced by the mentioned ablation patterns, we performed computational simulations of the resultant corneal shapes for the 13 eyes. For each particular cornea, we calculated the Munnerlyn ablation pattern $f_{\text{Mun}}(\rho, \theta)$, the parabolic ablation pattern $f_{\text{par}}(\rho, \theta)$ and the ablation pattern $f_{\text{bic}}(\rho, \theta)$ designed with biconics. These three ablation patterns were calculated for the same spherocylindrical correction, optical zone diameter, and central ablation depth used in surgery. In addition, the biconic ablation pattern was calculated in order to maintain the spherical aberration of each cornea. We also calculated a customized ablation pattern $f_{\text{cus}}(\mathbf{r})$ using Eq. (5) to correct for the individual ocular aberrations that were measured before surgery. The customized ablation pattern was designed with a 6.5-mm-diameter optical zone, the same area in which aberrations were measured.

We computed the resultant corneal elevation maps by subtracting the theoretical ablation depth from the measured preoperative corneal elevation at each point within the optical zone (using the corresponding correction for each eye). In other words, we performed a “computer surgery” on each preoperative “simulated cornea.” These computations were performed with software developed in Matlab (Mathworks, Natick, Mass.).

The Munnerlyn ablation pattern $f_{\text{Mun}}(\rho, \theta)$ and the parabolic ablation pattern $f_{\text{par}}(\rho, \theta)$ were calculated twice for each eye: first, centered at the corneal apex and second, centered in the pupil. The biconic ablation pattern $f_{\text{bic}}(\rho, \theta)$ was centered only at the corneal apex. The customized ablation pattern was centered in the pupil, which was the reference axis for the LRT total aberration measurements.

D. Corneal Asphericity from Corneal Height Data

For each eye we assessed the corneal asphericities before LASIK surgery (from measured preoperative topographies), after LASIK surgery (from measured postoperative topographies), and after “computer surgery” (from simulated corneal heights). We developed routines in

Table 1. Clinical Parameters Used for Surgery of All Eyes in the Study

Parameter	Eye Number												
	1	2	3	4	5	6	7	8	9	10	11	12	13
Spherical equivalent (D)	-2	-2.75	-3.25	-3.5	-5.375	-6.25	-6.25	-7.25	-7.25	-7.5	-7.5	-8.875	-11.5
Astigmatism (D)	1	0.5	1	1	0.75	1.5	1	1.5	1.5	1	1.5	1.75	2.5
Optical zone diameter (mm)	6.5	6.5	7	7	6	6.5	6	6	5	6	5	5	4.4
Central ablation depth (μm)	54	53	94	100	103	148	120	143	100	132	104	122	126

Matlab that used a least-mean-squares procedure to obtain the biconic $b(\rho, \theta; R_x, R_y, Q_x, Q_y, \theta_x, b_0)$ that best fit the corneal heights. We used biconics given by the following function¹⁶:

$$b(\rho, \theta; R_x, R_y, Q_x, Q_y, \theta_x, b_0) = b_0 - \frac{\rho^2 \left[\frac{\cos^2(\theta - \theta_x)}{R_x} + \frac{\sin^2(\theta - \theta_x)}{R_y} \right]}{1 + \left\{ 1 - \rho^2 \left[(Q_x + 1) \frac{\cos^2(\theta - \theta_x)}{R_x^2} + (Q_y + 1) \frac{\sin^2(\theta - \theta_x)}{R_y^2} \right] \right\}^{1/2}} \quad (6)$$

with six fitting free parameters $R_x, R_y, Q_x, Q_y, \theta_x, b_0$.

Corneal height data were expressed in cylindrical coordinates with (ρ_i, θ_i, h_i) , i.e., the radial, polar, and height coordinates for each of the points i provided by the corneal topography system, with $\rho = 0$ at the corneal apex. We used height data only within the optical zone, so the computed asphericities refer to the corneal shape within the optical zone.

The function $b(\rho, \theta; R_x, R_y, Q_x, Q_y, \theta_x, b_0)$ has a maximum at $\rho = 0$, where it takes the value b_0 . The radii of curvature of the surface at $\rho = 0$ are R_x and R_y in the directions defined respectively by $\theta = \theta_x$ and $\theta = \theta_x + \pi/2$. The profile along the direction $\theta = \theta_x$, which is described by the function $b(\rho, \theta_x; R_x, R_y, Q_x, Q_y, \theta_x, b_0)$, is a conic section with apical radius of curvature R_x and asphericity Q_x . Likewise, the curve described by $b(\rho, \theta_x + \pi/2; R_x, R_y, Q_x, Q_y, \theta_x, b_0)$ is a conic section with apical radius of curvature R_y and asphericity Q_y .

Positive asphericities describe oblate ellipsoids, and they get steeper as ρ increases. Asphericities less than zero and more than -1 describe prolate ellipsoids, which get flatter with increasing ρ . Conic sections with 0 asphericity are circumferences, and conic sections with -1 asphericity are parabolas.

We will denote the fitting parameters of the preoperative corneas and postoperative corneas as $(R_{x \text{ pre}}, R_{y \text{ pre}}, Q_{x \text{ pre}}, Q_{y \text{ pre}}, \theta_{x \text{ pre}}, b_{0 \text{ pre}})$ and $(R_{x \text{ post}}, R_{y \text{ post}}, Q_{x \text{ post}}, Q_{y \text{ post}}, \theta_{x \text{ post}}, b_{0 \text{ post}})$, respectively. We used $Q_{x \text{ pre}}, Q_{y \text{ pre}}$ and $Q_{x \text{ post}}, Q_{y \text{ post}}$ to assess the changes in asphericity induced by LASIK surgery. Likewise, theoretical changes in asphericity induced by the theoretical ablation patterns were assessed with the fitting parameters of simulated corneas. We compared changes theoretically induced by ablation patterns with real changes induced by surgery.

E. Corneal Aberrations from Corneal Topography

We obtained corneal aberrations of real preoperative corneas, real postoperative corneas, and simulated postoperative corneas. For this task, corneal elevations were exported to an optical design program (Zemax version 9; Focus Software, Tucson, Ariz.), which performed a ray-tracing simulation to compute corneal aberrations from corneal topography data. Corneal aberrations were calculated with the object point at infinity and the image point at corneal best focus. Wavelength was set to 543

nm (as in the LRT measurements). Corneal aberrations were expressed as a seventh-order Zernike polynomial expansion. This technique has been validated in previous studies in our laboratory.^{21,22}

F. Computation of Ablation Patterns

1. Munnerlyn Ablation Pattern

The Munnerlyn pattern assumes that the preoperative and postoperative corneal surfaces are spheres. As described in Eq. (1), the Munnerlyn function consists of the subtraction of the spherical surface with the attempted radius of curvature from the spherical surface that best fits the preoperative cornea [following the sign criterion used in the biconic function, Eq. (6)].

To include astigmatic correction, we extend Eq. (1) to a non-axially-symmetric pattern that considers corneas with astigmatism, that is, corneas with a different radius of curvature for each meridian θ . Then the biconic shapes described above will take the form of $b(\rho, \theta; R_x, R_y, 0, 0, \theta_x, 0)$, the sections of which are arcs of circumference with radii of curvature between R_x and R_y .

The Munnerlyn pattern will therefore be described by

$$f_{\text{Mun}}(\rho, \theta) = b(\rho, \theta; R_{x1}, R_{y1}, 0, 0, \theta_{x1}, 0) - b(\rho, \theta; R_{x2}, R_{y2}, 0, 0, \theta_{x2}, 0) + f_0, \quad (7)$$

where f_0 is the central ablation depth (we used the value supplied by the software controlling the laser system), $b(\rho, \theta; R_{x1}, R_{y1}, 0, 0, \theta_{x1}, 0)$ is the best spherocylindrical fit to the preoperative cornea with $(R_{x1}, R_{y1}, \theta_{x1}) = (R_{x \text{ pre}}, R_{y \text{ pre}}, \theta_{x \text{ pre}})$, and $b(\rho, \theta; R_{x2}, R_{y2}, 0, 0, \theta_{x2}, 0)$ is the attempted final corneal shape calculated to correct defocus and astigmatism. $(R_{x2}, R_{y2}, \theta_{x2})$ are computed as follows from the attempted spherical (S) and cylindrical (C) correction $S/C \times \alpha$ (S is the correction in diopters along the meridian of angle α , and $S + C$ is the correction along the meridian of angle $\alpha + \pi/2$). For each eye, we calculated the desired defocus and astigmatism $S_2/C_2 \times \alpha_2$ of the final cornea to correct for the total defocus and astigmatism. For each meridian, we assumed that the optical power of the final anterior cornea is the sum of the optical power of the initial anterior cornea and the attempted correction (negative for myopia) entered in the LASIK system during surgery. We used the dependence of the refractive power on the angle θ^7 :

$$S_2 + C_2 \sin^2(\theta - \alpha_2) = [S_1 + C_1 \sin^2(\theta - \alpha_1)] + [S + C \sin^2(\theta - \alpha)], \quad (8)$$

where $S_1/C_1 \times \alpha_1$ represents the defocus and astigmatism of the preoperative cornea and $S/C \times \alpha$ represents the defocus and astigmatic correction. S_1 , C_1 , and α_1 are calculated from $(R_{x1}, R_{y1}, \theta_{x1})$ by the following equations:

$$S_1 = \frac{n-1}{R_{x1}}, \quad C_1 = (n-1) \left(\frac{1}{R_{x1}} - \frac{1}{R_{y1}} \right),$$

$$\alpha_1 = \theta_{x1}, \quad (9)$$

where n is the refractive index of the cornea.

Finally, Eq. (9) were also used to obtain $(R_{x2}, R_{y2}, \theta_{x2})$ from $S_2/C_2 \times \alpha_2$. Because the orientations of corneal and total astigmatisms may be different, the desired corneal astigmatism could be not aligned with the preoperative astigmatism.

The sections of the function $f_{\text{Mun}}(\rho, \theta)$ along each meridian ($\theta = \text{constant}$) satisfy the Munnerlyn Eq. (1) and consist of the subtraction of the arc of circumference that represents the preoperative cornea along the meridian from the arc of circumference with the attempted radius of curvature for the meridian.

2. Parabolic Ablation Pattern

The parabolic ablation pattern can be obtained by truncating the Taylor expansion of the exact Munnerlyn function. Equation (4) is the parabola that corrects for a refractive error S . Astigmatism treatment involves a different refractive correction for each meridian ($\theta = \text{constant}$) and in the case of a parabolic ablation pattern, a different parabola for each meridian. Consequently, the parabolic ablation pattern designed to correct for defocus and astigmatism is a biconic, the sections of which are the parabolas that correct for the corresponding refractive error along each meridian:

$$f_{\text{par}}(\rho, \theta) = b \left(\rho, \theta; \frac{3}{8S}, \frac{3}{8(S+C)}, -1, -1, \alpha, f_0 \right). \quad (10)$$

As opposed to the Munnerlyn exact function $f_{\text{Mun}}(\rho, \theta)$, the parabolic ablation pattern $f_{\text{par}}(\rho, \theta)$ requires only f_0 and the sphero-cylindrical correction but not the apical radii of curvature of the preoperative cornea. We used the central ablation depth f_0 supplied by the software controlling the laser system.

3. Biconic Ablation Pattern

The biconic ablation pattern considers the preoperative and postoperative corneas as biconics. Apart from control of the postoperative radii of curvature, it also allows tuning of the postoperative asphericity. The biconic ablation pattern can therefore be computed as

$$f_{\text{bic}}(\rho, \theta) = b(\rho, \theta; R_{x1}, R_{y1}, Q_{x1}, Q_{y1}, \theta_{x1}, 0) \\ - b(\rho, \theta; R_{x2}, R_{y2}, Q_{x2}, Q_{y2}, \theta_{x2}, 0) \\ + f_0, \quad (11)$$

where f_0 is the central ablation depth, $b(\rho, \theta; R_{x1}, R_{y1}, Q_{x1}, Q_{y1}, \theta_{x1}, 0)$ is the best biconic fit to the preoperative cornea with $(R_{x1}, R_{y1}, Q_{x1}, Q_{y1}, \theta_{x1}) = (R_{x \text{ pre}}, R_{y \text{ pre}}, Q_{x \text{ pre}}, Q_{y \text{ pre}}, \theta_{x \text{ pre}})$, and

$b(\rho, \theta; R_{x2}, R_{y2}, Q_{x2}, Q_{y2}, \theta_{x2}, 0)$ is the attempted final corneal shape calculated to correct defocus and astigmatism and to maintain spherical aberration. $(R_{x2}, R_{y2}, \theta_{x2})$ are computed from the attempted spherical (S) and cylindrical (C) corrections as described in Eqs. (8) and (9), and Q_{x2} and Q_{y2} are computed as follows from the preoperative corneal spherical aberration. The primary spherical-aberration coefficient (fourth-order aberration) of a conicoid surface separating air and a medium of refractive index n can be expressed as⁷

$$w_4 = \frac{(n-1)(1+n^2Q)}{8R^3n^2}. \quad (12)$$

This expression was obtained considering the object point at infinity and the image point at the paraxial focus. The asphericity Q_{x2} was computed so that the coefficient w_4 calculated with R_{x2} and Q_{x2} takes the same value as that calculated with the apical radius of curvature and asphericity of the initial biconic surface along the meridian θ_{x2} . The same criterion was used to estimate Q_{y2} from the apical radius of curvature and asphericity of the initial biconic surface along the meridian $\theta_{x2} + \pi/2$. The apical radii of curvature and the asphericities of the initial biconic surface along the meridians θ_{x2} and $\theta_{x2} + \pi/2$ were calculated by using equations provided by Schwiegerling and Snyder.¹⁶ With this choice for Q_{x2} and Q_{y2} , we aimed at preserving the fourth-order aberrations. Another potential choice for the final asphericity could have been to cancel the total (internal plus corneal) spherical aberration.

4. Customized Ablation Pattern

Equation (5) was used to simulate a customized ablation pattern designed with the individual ocular aberrations measured by the LRT aberrometer before surgery. As opposed to the previous ablation patterns, the customized ablation pattern was calculated for a 6.5-mm pupil, i.e., the area where aberrations were measured:

$$f_{\text{cus}}(\rho, \theta) = \frac{W(\rho, \theta)}{n-1},$$

$$W(\rho, \theta) = \sum_{n=0}^7 \sum_m C_n^m Z_n^m(\rho, \theta). \quad (13)$$

The wave-front aberration $W(\rho, \theta)$ was obtained from LRT measurements. C_n^m denote the Zernike coefficients in the OSA standard notation.

In all these computations, central ablation depth f_0 (a constant value) does not influence the resultant aberrations or biconic fitting.

3. RESULTS

A. Preoperative and Postoperative Asphericities

Figures 2 and 3 show asphericities Q_x and Q_y of the real corneas before and after LASIK surgery. Eyes in Figs. 2 and 3 are sorted by increasing preoperative spherical error. Mean preoperative corneal asphericity was -0.14 ± 0.14 (standard deviation), which is close to the value (-0.16) found by Holladay *et al.*⁸ in a study with 14 myo-

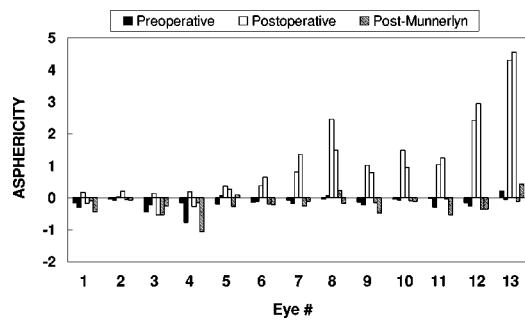


Fig. 2. Asphericities (Q_x , first column, and Q_y , second column) of the biconic surfaces that best fit the corneal heights within each individual optical zone for preoperative and postoperative real corneal topographies and for simulated corneas with the Munnerlyn pattern centered at the corneal apex. Patients are sorted by increasing correction, as in Table 1.

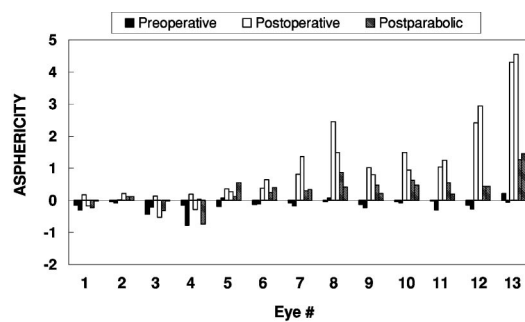


Fig. 3. As Fig. 2, but with the parabolic pattern.

pic eyes. Mean postoperative asphericities (1.1 ± 1.3) were positive (oblate corneas) and much higher than preoperative asphericities. Postoperative asphericity was correlated with preoperative spherical error ($r = 0.91$, $p < 0.0001$). Preoperative and postoperative asphericities were slightly but statistically significantly correlated ($r = 0.6$, $p = 0.03$).

B. Post-Munnerlyn Asphericities

The simulations with the Munnerlyn ablation pattern did not produce the increased asphericities that were found in real corneas after surgery. Figure 2 shows the corneal asphericities Q_x and Q_y before and after surgery and after the computer simulations of the Munnerlyn ablation pattern centered at the corneal apex.

The asphericities of the simulated corneas were on average -0.21 ± 0.19 , and were correlated with preoperative asphericities ($r = 0.98$, $p < 0.0001$), for the Munnerlyn pattern centered at the corneal apex. In corneas with negative preoperative asphericities along the two principal meridians, both post-Munnerlyn asphericities decreased (i.e., eyes 3, 4, 9, and 12). If one of them was positive, the simulation produced one increased positive asphericity along one meridian and one decreased negative asphericity along the other meridian (i.e., eyes 5, 8, and 13). In corneas with asphericities close to 0, the Munnerlyn ablation pattern did not induce any significant change (i.e., eyes 2 and 10). These effects also depended on the magnitude of the treatment: The higher the myopic correction, the larger the change in asphericity after Munnerlyn simulation. For example, although

eyes 5 and 8 have the same positive preoperative asphericity along one of the principal meridians ($Q_{pre} = 0.07$), the corresponding increased positive asphericity after the subtraction of the Munnerlyn function is higher in eye 8 ($Q_{Mun} = 0.23$) than in eye 5 ($Q_{Mun} = 0.10$), which was treated with a lower correction.

Centering the Munnerlyn pattern in the pupil produced a mean asphericity of the simulated corneas of -0.2 ± 0.3 , very close to the mean asphericity obtained when the ablation pattern was centered at the corneal apex. In this case, simulated post-Munnerlyn asphericities were also significantly correlated with initial asphericities ($r = 0.60$, $p = 0.03$), although not as strongly as in the case of the pattern centered at the corneal apex.

C. Postparabolic Asphericities

Figure 3 compares the real preoperative and postoperative asphericities with the simulated postparabolic asphericities. In this case, simulated asphericities increased regardless of whether preoperative asphericities were negative or positive. Mean asphericity of the simulated corneas was 0.3 ± 0.4 when the ablation pattern was centered at the corneal apex and 0.4 ± 0.5 when the ablation pattern was centered in the pupil. Unlike what was found for the simulations of the exact Munnerlyn ablation pattern, and following the trend of clinical postoperative asphericities, the largest increase in asphericity was found in eyes with high preoperative spherical error.

In addition, we found a correlation between the simulated postparabolic asphericity and the preoperative asphericity ($r = 0.84$, $p < 0.0001$) when the ablation pattern was centered at the corneal apex, as well as when the ablation pattern was centered in the pupil ($r = 0.81$, $p = 0.0003$). The higher the preoperative asphericity, the higher the simulated postparabolic asphericity. As an example to illustrate the dependence on preoperative asphericity, eyes 8 and 9 have the same spherical equivalent and astigmatism corrections, but the preoperative mean asphericity was higher in eye 8 ($Q_{pre} = 0.01$) than in eye 9 ($Q_{pre} = -0.18$). The mean asphericity of the simulated corneas was higher in eye 8 ($Q_{par} = 0.64$) than in eye 9 ($Q_{par} = 0.34$) with the pattern centered at the corneal apex.

D. Spherical Aberration of Real Corneas after Standard LASIK Surgery and of Simulated Corneas with the Standard Ablation Patterns

Corneal spherical aberrations were calculated for a 4.4-mm pupil centered at the corneal apex. Changes in corneal spherical aberrations parallel changes in corneal asphericities. Figures 4(a) and 4(b) show that standard myopic LASIK induced positive corneal spherical aberration and that the magnitude of this aberration increased with attempted correction. The mean C_4^0 Zernike coefficient increased from $0.08 \pm 0.04 \mu\text{m}$ to $0.17 \pm 0.10 \mu\text{m}$ in real eyes. However, the predicted mean C_4^0 from the computer simulations with the standard ablation patterns centered at corneal apex was $0.05 \pm 0.03 \mu\text{m}$ for the Munnerlyn formula and $0.11 \pm 0.04 \mu\text{m}$ for the parabolic formula. In general, C_6^0 Zernike coefficients were one order of magnitude less than C_4^0 , and therefore C_4^0 coefficients are the main contribution to the root mean square

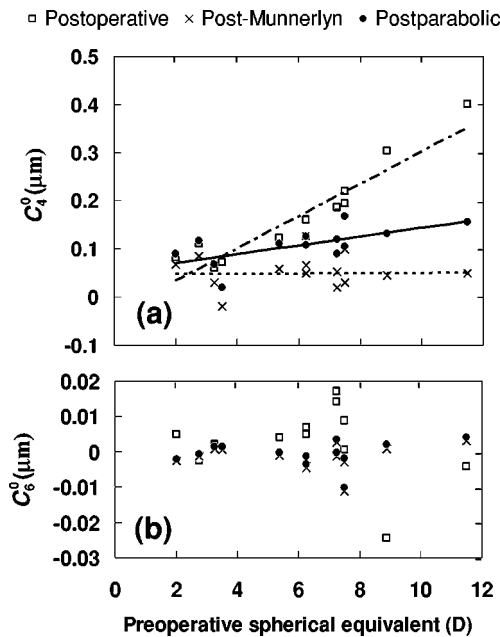


Fig. 4. (a) Fourth-order spherical-aberration Zernike coefficient C_4^0 and (b) sixth-order spherical aberration Zernike coefficient C_6^0 for real postoperative corneas and for simulated post-Munnerlyn and postparabolic corneas. In these simulations the theoretical ablation patterns were calculated centered at the corneal apex. Data are for a 4.4-mm pupil.

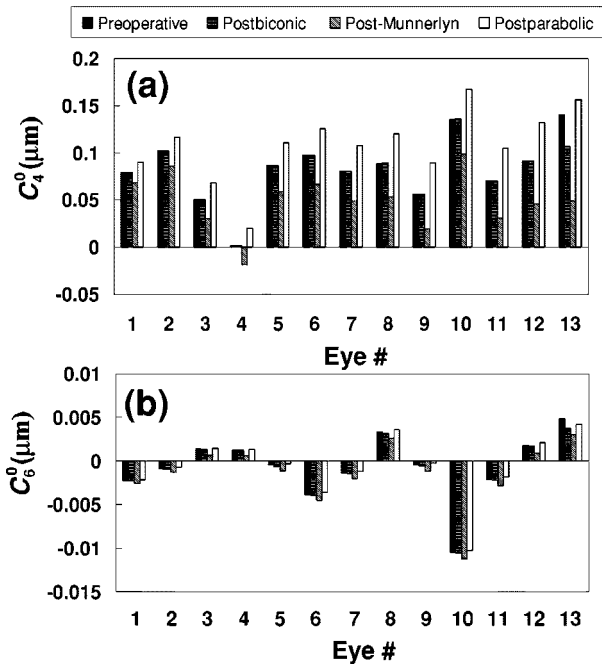


Fig. 5. (a) Fourth-order spherical-aberration Zernike coefficient C_4^0 and (b) sixth-order spherical aberration Zernike coefficient C_6^0 for real preoperative corneas and for simulated post-Munnerlyn, postparabolic, and postbiconic corneas. In these simulations the theoretical ablation patterns were calculated centered at the corneal apex. Data are for a 4.4-mm pupil.

(RMS) of the spherical aberration. As seen in Fig. 4(a), the corneal spherical aberration after standard myopic LASIK is highly correlated with the preoperative spherical equivalent error: slope = $0.03 \mu\text{m D}^{-1}$, $r = 0.93$ ($p < 0.0001$). However, the predictions from the computer

simulations did not show any correlation between the post-Munnerlyn spherical aberration and the preoperative spherical-equivalent error: $r = 0.03$ ($p = 0.92$). There is a low but statistically significant correlation between the postparabolic spherical aberration of the simulated corneas and the preoperative spherical error: slope = $0.0091 \mu\text{m D}^{-1}$, $r = 0.65$ ($p = 0.01$).

E. Biconic Ablation Pattern

Figure 5 demonstrates that the ablation pattern designed with biconic surfaces was successful at maintaining corneal spherical aberration, which was our goal when deciding the final biconic surface asphericities. Although our imposition was intended to maintain w_4 Seidel spherical aberration, spherical-aberration Zernike coefficients remained almost constant. Figure 5 shows that spherical aberration is decreased by the Munnerlyn pattern, maintained constant by the biconic pattern, and increased by the parabolic pattern in every eye. Hence the biconic ablation pattern is in between the Munnerlyn and the parabolic formulas.

F. Customized Ablation Pattern

The aim of the customized ablation pattern designed with the wave aberration $W(\rho, \theta)$ is to reduce the optical path lengths of the rays incoming the cornea by the values of $W(\rho, \theta)$. This should produce a change in aberrations of the anterior corneal surface such that the postoperative corneal aberrations will compensate the internal aberrations. This theoretical formulation assumes that the internal aberrations do not change with surgery.

Total (internal plus corneal) aberrations generated theoretically by the customized ablation pattern can be calculated as the differences between $W(\rho, \theta)$ and the simulated change of corneal aberrations. For a perfect optical correction these differences should equal zero. The simulated change in corneal aberrations was calculated as the aberrations of the simulated postcustomized cornea minus the aberrations of the real preoperative cornea.

Simulations of the customized ablation pattern induced a nonzero total spherical aberration that was correlated with correction ($r = 0.968$; $p < 0.0001$, Fig. 6) and with the preoperative total spherical aberration ($r = 0.798$, $p = 0.001$). Figure 7(a) shows that third-order aberrations

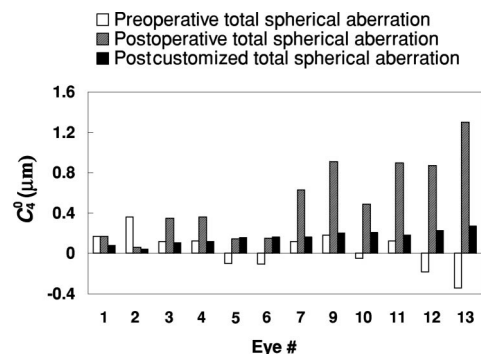


Fig. 6. Zernike coefficient C_4^0 of the total (internal plus corneal) aberrations from the preoperative and postoperative LRT aberrometry measurements and from the computer simulations of the customized ablation. Data are for a 6.5-mm pupil.

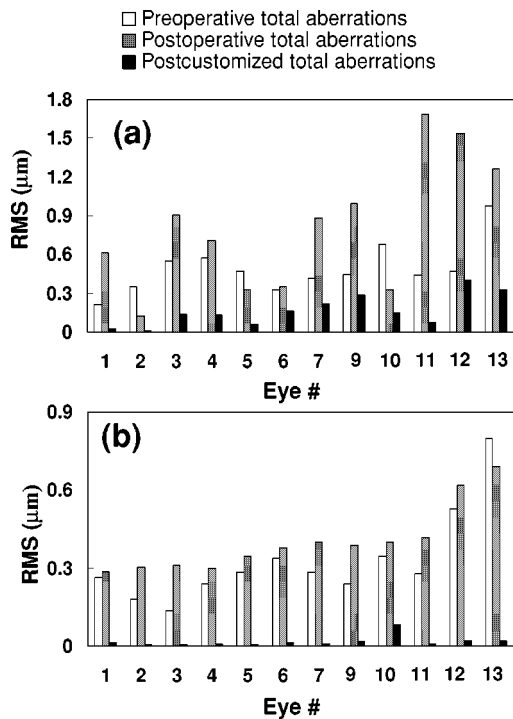


Fig. 7. RMS (a) of the total (internal plus corneal) third-order aberrations and (b) of the total fourth-and-higher-order asymmetric aberrations from the preoperative and postoperative LRT aberrometry measurements and from the computer simulations of the customized ablation. Data are for a 6.5-mm pupil.

tions (coma) were not completely corrected by the theoretical customized formula. Mean RMS of the third-order total aberrations decreased from $0.5 \pm 0.2 \mu\text{m}$ to $0.2 \pm 0.1 \mu\text{m}$. Postoperative total aberrations were also correlated with correction ($r = 0.768, p = 0.002$). On the other hand, Fig. 7(b) shows that fourth-and-higher-order asymmetric total aberrations were successfully corrected (fourth-and-higher-order asymmetric Zernike coefficients changed from $0.3 \pm 0.2 \mu\text{m}$ to $0.02 \pm 0.02 \mu\text{m}$ with the theoretical customized formula).

4. DISCUSSION

A. Comparison of Our Computational Study with Previous Studies

Post-Munnerlyn asphericities from our simulations depend on both preoperative asphericities and refractive correction in the same way as Gatinel *et al.*¹⁴ found in their calculations. These authors used the exact Munnerlyn formula [Eq. (3)] and a numerical procedure to calculate final asphericities. In addition, the postparabolic asphericities from our simulations are very similar to those predicted by the formula provided by Jiménez *et al.*,¹³ who carried out analytical calculations with the parabolic approximation [Eq. (4)] of the Munnerlyn function. In both studies, preoperative corneas were simulated with ideal conicoid surfaces instead of topographic data from real patients as in our simulations.

Our computer simulations solve the discrepancy created by these two studies. Although Gatinel *et al.*¹⁴ used the exact Munnerlyn formula, they used only 31 points along the radial distance of the computed surfaces to cal-

culate their asphericities. On the other hand, Jiménez *et al.*¹³ asserted that differences between the exact Munnerlyn formula and the parabolic approximation are negligible (at most 5%). Therefore it remained unexplained whether the discrepancies between the results of these two studies were due to the numerical procedure used by Gatinel *et al.*¹⁴ or to the differences between the exact and the parabolic formulas. The results from our computer simulations show that differences introduced by approximating to a parabola in the Munnerlyn exact formula have an important effect on the induced corneal spherical aberration.

Gatinel *et al.*¹⁴ also found a slight dependence of post-Munnerlyn asphericities on preoperative apical radius of curvature, but this dependence is negligible when compared with the dependence on preoperative asphericity or refractive correction.

This finding has an intuitive interpretation. We can understand LASIK myopic ablation as removal of a positive lens from the cornea. If the surfaces of the removed lens are less prolate than the preoperative corneal shape (i.e., Munnerlyn ablation), asphericity should decrease, but if the surfaces of the removed lens are more prolate than the cornea (e.g., parabolic ablation), asphericity should increase. This explains the finding that parabolic ablation patterns increase positive corneal spherical aberrations and that Munnerlyn ablation patterns reduce the spherical aberration in most cases (since preoperative corneas usually are prolate).

B. Causes of Discrepancies between Theoretical Computations and Real Data

Our results show that the increase in asphericity (and spherical aberration) induced by standard LASIK surgery is much higher than that generated by the theoretical Munnerlyn ablation pattern, especially for high myopic corrections. In fact, the theoretical Munnerlyn pattern not only does not induce corneal spherical aberration but reduces it slightly. Measurements of ablated polymethyl methacrylate surfaces by Dorrnsoro *et al.*²³ suggest that the standard ablation algorithms programmed into the laser systems are based on the parabolic ablation pattern. Our simulations show that the theoretical parabolic pattern could account for a part (40%) of the increase in asphericity found clinically, but there must be additional factors that explain the systematic increase of asphericity induced by standard LASIK surgery.

1. Reflection Losses and Nonnormal Incidence

Reflection losses and nonnormal incidence of the laser radiation onto the cornea have often been invoked to explain discrepancies between the Munnerlyn ablation pattern and the actual pattern sculpted on the cornea.^{17,24} Both effects cause a reduction of the absorbed energy density that varies with the angle of incidence. As the laser pulses move from the corneal apex to the periphery the angle of incidence increases, and consequently the absorbed energy density decreases, for two reasons. First, Fresnel's laws predict that reflected energy increases as the angle of incidence increases. Second, the illuminated spot area on the corneal surface gets larger at the periphery, decreasing the energy density.

The ablation threshold is the minimum energy density needed to remove tissue and has been studied for the human cornea at 193 nm of the argon fluoride excimer laser. The value for this threshold varies among studies^{25–28} between 30 and 50 mJ/cm². For absorbed energy densities above the ablation threshold, the ablation depth per pulse depends on the energy density following a logarithmic trend,^{29,30}

$$d = m \log(F/F_{\text{th}}), \quad F \geq F_{\text{th}}, \quad (14)$$

where d is the ablation depth per pulse when the absorbed energy density is F (mJ/cm²), F_{th} is the ablation threshold, and m is a constant. The higher the absorbed energy density, the deeper the ablation. Because the absorbed energy density is lower at the periphery, the ablation efficiency diminishes as we move from the apex to the periphery. Jiménez *et al.*¹⁷ performed analytical calculations to estimate how both reflection losses and nonnormal incidence modify the final corneal shape. They assumed a homogeneous spot, nonpolarized light, and Fresnel's laws and provided an adjustment factor to multiply the ablation-pattern function:

$$K(\phi) = 1 + a \log\{[1 - R(\phi)]\cos \phi\}, \quad (15)$$

where $a = 1/\log(F_0/F_{\text{th}})$, ϕ is the angle of incidence and $R(\phi)$ is the reflectivity from Fresnel's laws. F_0 is the energy density delivered by the laser system. Reflectivity was calculated by using a refractive index of 193 nm for $n = 1.52$ (neglecting the imaginary part).³¹ The factor $K(\phi)$ can take values between 0 and 1.

To quantify how reflection losses and nonnormal incidence could modify the postoperative corneal shape, we incorporated the factor $K(\phi)$ into our “computer surgery” for both Munnerlyn and parabolic ablation patterns. The computer surgery considering reflection losses and nonnormal incidence consists of subtracting from the preoperative corneal heights the ablation patterns multiplied by the factor $K(\phi)$: $f_{\text{Mun}}(\rho, \theta)K(\phi)$ and $f_{\text{par}}(\rho, \theta)K(\phi)$ for the Munnerlyn and the parabolic ablation patterns, respectively. For these simulations we used $a = 1.14$ in Eq. (15). This value is calculated from the energy density delivered by the LASIK system ($F_0 = 120$ mJ/cm²) and from the highest ablation threshold found in literature ($F_{\text{th}} = 50$ mJ/cm²). The higher the ablation threshold, the larger the modifications induced by reflection losses and nonnormal incidence. We used the highest ablation threshold to estimate the largest expected effect of this effect on corneal asphericity.

Figure 8 shows an example of Munnerlyn and parabolic ablation patterns considering and not considering reflection losses and nonnormal incidence. The plotted functions are the ablation patterns for eye 3 across the $\alpha + \pi/2$ meridian, i.e., functions $f_{\text{Mun}}(\rho, \alpha + \pi/2)$, $f_{\text{par}}(\rho, \alpha + \pi/2)$, $f_{\text{Mun}}(\rho, \alpha + \pi/2)K(\phi)$, and $f_{\text{par}}(\rho, \alpha + \pi/2)K(\phi)$ with the specific parameters for this eye (see Table 1).

Computer simulations show that reflection losses and nonnormal incidence induce changes in both radii of curvature and asphericities of the resultant simulated corneas. Figure 9 shows that the theoretical Munnerlyn ablation pattern was achieved to correct for preoperative defocus when changes in ablation efficiency were not con-

sidered. However, simulated corneas became overcorrected when reflection losses and nonnormal incidence were taken into account (the mean remaining spherical equivalent was -0.46 D \pm 0.13 D). Asphericity increased in all the simulated resultant corneas when reflection losses and nonnormal incidence were considered (Fig. 10). The increase in asphericity due to reflection losses and nonnormal incidence (discounting the changes in asphericity induced by the ablation pattern on its own) was 0.5 ± 0.3 for the Munnerlyn ablation pattern and 0.4 ± 0.3 for the parabolic ablation pattern. The most detrimental effect is the increase of asphericity, because overcorrection can be corrected by changing the nomogram in the LASIK system program.

Changes introduced by reflection losses and nonnormal incidence near the center of the ablation pattern account for the overcorrection of the simulated resultant corneas (see Fig. 8). Changes in the ablation patterns in the periphery are also necessary to justify the resultant asphericities.

Central ablation depth $f_0 = f_0^{\text{OZ}} + f_0^{\text{TZ}}$ did not affect the shape of the simulated resultant corneas when reflection losses and nonnormal incidence were ignored. In simu-

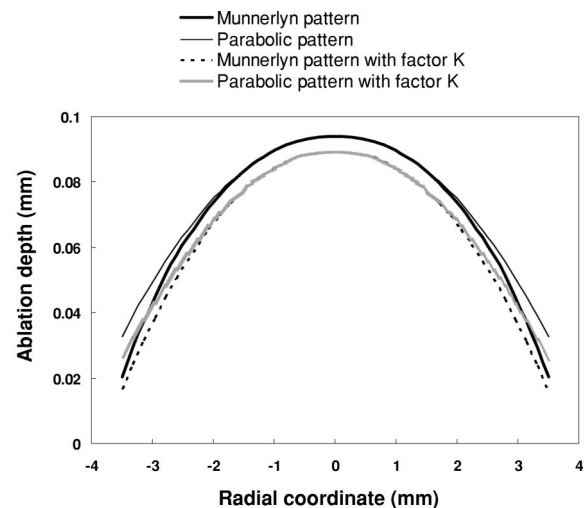


Fig. 8. Munnerlyn and parabolic patterns considering and not considering reflection losses and nonnormal incidence with the model provided by Jiménez *et al.*¹⁷ The represented ablation-pattern section corresponds to eye 3 along the meridian of correction -3.75 D within the optical zone.

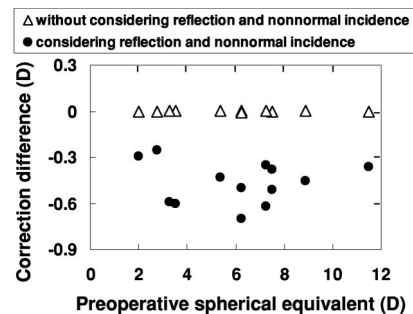


Fig. 9. Obtained minus attempted spherical-equivalent correction versus preoperative spherical-equivalent correction for the Munnerlyn pattern considering and not considering reflection losses and nonnormal incidence with the model described by Jiménez *et al.*¹⁷

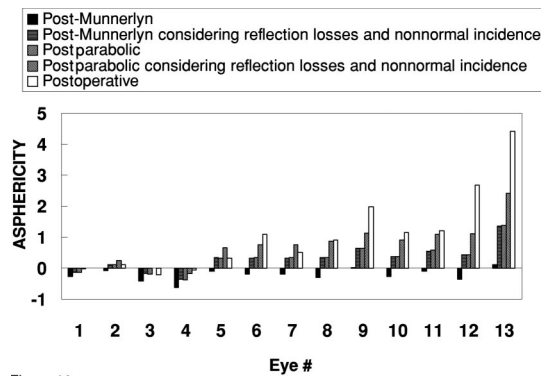


Fig. 10. Mean asphericities $(Q_x + Q_y)/2$ of the biconic surfaces that best fit the corneal heights within each individual optical zone for postoperative real corneal topographies and for post-Munnerlyn and postparabolic simulated corneas considering and not considering both reflection and nonnormal incidence. Patients are sorted by increasing correction, as in Table 1.

lations without the factor $K(\alpha)$, the central ablation depth f_0 was subtracted from preoperative corneal topographies as a constant value at every point [see Eqs. (7), (10), and (11)]. However, in simulations with the factor $K(\alpha)$, the effective depth was no longer constant, and it changed as a function of corneal position, $f_0K(\alpha)$, therefore affecting the resultant corneal shape. As a consequence, patients with the same correction could have different results because of different ablation depths. For this reason, we used the central ablation depths supplied by the PlanoScan program for each eye. This is an advantage of our individual “computer surgery” over other analytical calculations that used the exact expression of f_0^Z rather than the actual value f_0 .

2. Limitations and Other Potential Causes of Discrepancy

Although a combination of parabolic approximation and changes in ablation efficiency produces asphericities that are closer to postoperative values, a part of the clinical increase in asphericity remains unexplained (40% for the eyes with preoperative spherical error higher than 7 D).

First, although the standard algorithms are nominally based on the Munnerlyn equation, these are proprietary, and the actual profile programmed into the laser system may show discrepancies from the theoretical formulation. The fact that typically only the attempted correction and the optical zone diameter, and not the radii of curvature, are required by the LASIK system may be indicative that a parabolic approximation of the Munnerlyn equation is being issued. Also, experiments using polymethyl methacrylate models suggest that a profile closer to a parabolic approximation is being used.²³

Second, surgery may affect corneal hydration, and the ablation depth per laser pulse on the cornea depends on the hydration state.³² Third, the wound-healing process³³ and the mechanical response of the cornea to ablation are not completely understood.

C. Customized Ablation Pattern

Our simulations account for changes only in corneal shape and corneal spherical aberration. Predictions about the postoperative total aberrations after custom-

ized ablation require the assumption that internal aberrations do not change with surgery. However, internal aberrations (computed as total minus corneal aberrations) are likely to shift as a result of changes on the posterior corneal surface and also because of a shift of the corneal best focus (or alternatively, changes in the convergence of rays on the crystalline lens). Our simulations (Fig. 6) show that the induced corneal spherical aberration with use of Eq. (5) does not match the expected outcome. We found residual spherical aberration and third-order aberrations that were correlated with the preoperative spherical equivalent (Fig. 7). This results from the fact that the corneal aberrations are estimated on the basis of the best preoperative corneal focus, but surgery induces a shift in the corneal focus. Although the customized ablation pattern is designed to correct for the wave aberration $W(\rho, \theta)$, when correcting for defocus the corneal focus changes, and consequently an additional corneal spherical aberration is induced.

Although fourth-and-higher-order asymmetric aberrations seem to be corrected by the theoretical ablation pattern, the resultant total spherical aberration was of the same order of magnitude as the preoperative total spherical aberration. Besides, only the 70% of the preoperative total coma is corrected by the theoretical ablation pattern.

D. Implications for Customized Refractive Surgery

The fact that the theoretical ablation patterns do not modify corneal asphericity significantly (and therefore do not induce the dramatic increase in spherical aberration found clinically) indicates that improvement in refractive surgery outcomes should rely not so much on a refinement of the theoretical design of the ablation patterns but on increasing the understanding of the reasons (e.g., application of the algorithm and wound healing and biomechanical response) for the increase in asphericity. We have shown that the biconic ablation pattern controls for both defocus and spherical aberration. The customized ablation pattern reduces high-order aberrations as well except for spherical aberration. However, these theoretical profiles should incorporate weighting factors that account for the changes in laser efficiency across the cornea and other biomechanical and healing factors. We need a better understanding of these factors to apply these findings across subjects and ablation profiles.

5. CONCLUSIONS

We have shown the effects of standard LASIK on corneal asphericity in comparison with the theoretical changes predicted by simulations of ablation patterns on real corneas. There are large discrepancies between clinical data and predictions of postoperative corneal asphericity and aberrations. A parabolic approximation of the standard Munnerlyn ablation pattern predicts a trend toward increased asphericity and spherical aberration, but significantly less than that shown by the clinical data. A biconic ablation pattern could control for spherical aberration. A customized ablation pattern based on individual wave-aberration measurements could compensate for high-order aberrations, although further studies are necessary to achieve control of coma and spherical aberration

when correcting defocus. On the other hand, we have demonstrated that changes in ablation efficiency across the cornea are not negligible, so they, too, have to be considered when designing any ablation algorithm. In addition, it is necessary to find other causes of increased asphericity to fully explain the clinical results and to design customized ablation algorithms that take such causes into account. Successful results from newly designed algorithms will rely on the proper considerations of laser efficiency and corneal biomechanics.

ACKNOWLEDGMENTS

The authors acknowledge funding from grants BFM2002-02638 from Ministerio de Ciencia y Tecnología, Spain and CAM08.7/004.1/2003 from Comunidad Autónoma de Madrid to S. Marcos. D. Cano was funded by a fellowship from Comunidad Autónoma de Madrid and S. Barbero by a fellowship from Ministerio de Ciencia, Cultura y Deporte, Spain. The authors thank J. Merayo-Llives (Instituto de Oftalmobiología Aplicada de Valladolid, Unidad Asociada Consejo Superior de Investigaciones Científicas) for helpful discussions.

Corresponding author Susana Marcos's e-mail address is susana@io.cfmac.csic.es; phone, 34-9156-16800; fax, 34-9156-45557.

REFERENCES

- I. Pallikaris, M. Papatzanaki, E. Stathi, O. Frenschok, and A. Georgiadis, "Laser in situ keratomileusis," *Lasers Surg. Med.* **10**, 463–468 (1990).
- S. Farah, D. Azar, C. Gurdal, and J. Wong, "Laser in situ keratomileusis: literature review of a developing technique," *J. Cataract Refract. Surg.* **24**, 989–1006 (1998).
- D. Huang and M. Arif, "Spot size and quality of scanning laser correction of higher-order wavefront aberrations," *J. Cataract Refract. Surg.* **28**, 407–416 (2002).
- S. Marcos, B. Barbero, L. Llorente, and J. Merayo-Llives, "Optical response to LASIK for myopia from total and corneal aberration measurements," *Invest. Ophthalmol. Visual Sci.* **42**, 3349–3356 (2001).
- E. Moreno-Barriuso, J. Merayo-Llives, S. Marcos, R. Navarro, L. Llorente, and S. Barbero, "Ocular aberrations before and after myopic corneal refractive surgery: LASIK-induced changes measured with laser ray tracing," *Invest. Ophthalmol. Visual Sci.* **42**, 1396–1403 (2001).
- B. Seitz, F. Torres, A. Langenbucher, A. Behrens, and E. S. Suarez, "Posterior corneal curvature changes after myopic laser in situ keratomileusis," *Ophthalmology* **108**, 666–672 (2001).
- G. Smith and D. A. Atchison, *The Eye and Visual Optical Instruments* (Cambridge U. Press, Cambridge, UK, 1997).
- J. T. Holladay, D. R. Dudeja, and J. Chang, "Functional vision and corneal changes after laser in situ keratomileusis determined by contrast sensitivity, glare testing and corneal topography," *J. Cataract Refract. Surg.* **25**, 663–669 (1999).
- S. MacRae, "Excimer ablation design and elliptical transition zones," *J. Cataract Refract. Surg.* **25**, 1191–1197 (1999).
- J. Schwiegerling, R. Snyder, and S. MacRae, "Optical aberrations and ablation pattern design," in *Customized Corneal Ablation: The Quest for Super Vision*, S. MacRae, R. Krueger, and R. Applegate, eds. (Slack, Inc. Thorofare, N.J., 2001), pp. 96–107.
- C. Munnerlyn, S. Koons, and J. Marshall, "Photorefractive keratectomy: a technique for laser refractive surgery," *J. Cataract Refract. Surg.* **14**, 46–52 (1988).
- J. Lin, "Critical review on refractive surgical lasers," *Opt. Eng.* **34**, 668–675 (1995).
- J. Jiménez, R. Anera, and L. Jiménez del Barco, "Equation for corneal asphericity after corneal refractive surgery," *J. Refract. Surg.* **29**, 65–69 (2003).
- D. Gatinel, T. Hoang-Xuan, and D. Azar, "Determination of corneal asphericity after myopia surgery with the excimer laser: a mathematical model," *Invest. Ophthalmol. Visual Sci.* **42**, 1736–1742 (2001).
- F. Manns, A. Ho, J. Parel, and W. Culbertson, "Ablation profiles for wavefront-guided correction of myopia and primary spherical aberration," *J. Cataract Refract. Surg.* **28**, 766–774 (2002).
- J. Schwiegerling and R. Snyder, "Custom photorefractive keratectomy ablations for the correction of spherical and cylindrical refractive error and higher-order aberration," *J. Opt. Soc. Am. A* **15**, 2572–2579 (1998).
- J. R. Jiménez, R. Anera, L. Jiménez del Barco, and E. Hita, "Effect on laser-ablation algorithms of reflection losses and nonnormal incidence on the anterior cornea," *Appl. Phys. Lett.* **81**, 1521–1523 (2002).
- E. Moreno-Barriuso, S. Marcos, R. Navarro, and S. A. Burns, "Comparing laser ray tracing, spatially resolved refractometer and Hartmann–Shack sensor to measure the ocular wavefront aberration," *Optom. Vision Sci.* **78**, 152–156 (2001).
- R. Navarro and E. Moreno-Barriuso, "Laser ray-tracing method for optical testing," *Opt. Lett.* **24**, 1–3 (1999).
- L. N. Thibos, R. A. Applegate, J. T. Schwiegerling, R. H. Webb, and V. S. T. Members, "Standards for reporting the optical aberrations of eyes," in *Vision Science and Its Applications*, Vol. 35 of OSA Trends in Optics and Photonics Series (Optical Society of America, Washington, D.C., 2000), pp. 110–130.
- S. Barbero, S. Marcos, and J. M. Merayo-Llives, "Total and corneal aberrations in an unilateral aphakic subject," *J. Cataract Refract. Surg.* **28**, 1594–1600 (2002).
- S. Barbero, S. Marcos, J. Merayo-Llives, and E. Moreno-Barriuso, "Validation of the estimation of corneal aberrations from videokeratography in keratoconus," *J. Refract. Surg.* **18**, 263–270 (2002).
- C. Dorransoro, D. Cano, S. Barbero, J. Merayo, L. Llorente, and S. Marcos, "Understanding the standard algorithm for corneal refractive surgery using laser ablation of PMMA surfaces," ARVO E-abstract 2535 (2003).
- M. Mrochen and T. Seiler, "Influence of corneal curvature on calculation of ablation patterns used in photorefractive laser surgery," *J. Refract. Surg. (Suppl.)* **17**, S584–S587 (2001).
- M. Berns, L. Chao, A. Giebel, L.-H. Liaw, J. Andrews, and B. VerSteege, "Human corneal ablation threshold using the 193-nm ArF excimer laser," *Invest. Ophthalmol. Visual Sci.* **40**, 826–830 (1999).
- R. Krueger, T. Seiler, T. Gruchman, M. Mrochen, and M. Berlin, "Stress wave amplitudes during laser surgery of the cornea," *Ophthalmology* **108**, 1070–1074 (2001).
- O. Kermani, H. Koort, E. Roth, and M. Dardenne, "Mass spectroscopic analysis of excimer laser ablated material from human corneal tissue," *J. Cataract Refract. Surg.* **14**, 638–641 (1988).
- C. Puliafito, R. Steinert, T. Deutsch, F. Hillenkamp, E. Dehm, and C. Adler, "Excimer laser ablation of the cornea and lens," *Ophthalmology* **92**, 741–748 (1985).
- R. Srinivasan, "Ablation of polymers and biological tissue by ultraviolet lasers," *Science* **234**, 559–565 (1986).
- T. Seiler and P. McDonnell, "Excimer laser photorefractive keratectomy," *Surv. Ophthalmol.* **40**, 89–118 (1995).
- G. Pettit and M. Ediger, "Corneal-tissue absorption coefficients for 193- and 213-nm ultraviolet radiation," *Appl. Opt.* **35**, 3386–3391 (1996).
- P. Dougherty, K. Wellish, and R. Maloney, "Excimer laser ablation rate and corneal hydration," *Am. J. Ophthalmol.* **118**, 169–176 (1994).
- D. Huang, T. Maolong, and R. Shekhar, "Mathematical model of corneal surface smoothing after laser refractive surgery," *Am. J. Ophthalmol.* **135**, 267–278 (2003).